Letter: New boundary layer structures due to strong wall slippage

Cite as: Phys. Fluids **30**, 121702 (2018); https://doi.org/10.1063/1.5078664
Submitted: 27 October 2018 . Accepted: 04 December 2018 . Published Online: 21 December 2018

Hideki Fujioka (藤岡秀樹), and Hsien-Hung Wei (魏憲鴻)

Letter: New boundary layer structures due to strong wall slippage

Hideki Fujioka (藤岡秀樹)[1] and Hsien-Hung Wei (魏憲鴻)[2,a)]
[1]*Center for Computational Science, Tulane University, New Orleans, Louisiana 70018, USA*
[2]*Department of Chemical Engineering, National Cheng Kung University, Tainan 701, Taiwan*

(Received 27 October 2018; accepted 4 December 2018; published online 21 December 2018)

In a laminar boundary layer flow, the extent of slip is not fixed but varies with the slip length λ relative to the boundary layer thickness δ. Here, we report that distinct boundary layer structures can arise from slip effects when λ exceeds δ. This is demonstrated by revisiting two closely related problems in the presence of wall slip: (i) the Stokes 1st problem and (ii) a steady high Reynolds number boundary layer flow driven by a moving plate (of length L). In (i), the wall stress is found to be constant for $\delta \ll \lambda$ for short times and persists until time t reaches the *slip-stick transition* (SST) point $t_\lambda \sim \lambda^2/\nu$ (with ν being the kinematic viscosity) after which the usual no-slip result $t^{-1/2}$ takes over. A similar transition can also occur spatially to (ii). We show that the boundary layer can turn from the thicker one $\delta \sim LRe^{-1/2} \gg \lambda$ in the weak-slip regime to the thinner one $\delta \sim L(\lambda/L)^{1/3}\, Re^{-1/3} \ll \lambda$ in the strong-slip regime. This boundary layer structure change is also accompanied by a shift from the well-known no-slip friction law $C_f \sim Re^{-1/2}$ to the strong-slip law $C_f \sim (L/\lambda)Re^{-1}$ when increasing the Reynolds number $Re = UL/\nu$ beyond the SST point $Re_c \sim (L/\lambda)^2$. Generalization to the Falkner-Skan wedge flow is also made, suggesting that similar friction law and boundary layer structure changes might occur in a wide class of wall-bounded boundary layer flows. *Published by AIP Publishing.* https://doi.org/10.1063/1.5078664

When solving fluid mechanics problems, the no-slip boundary condition is often imposed on solid boundaries. However, in situations involving hydrophobic/textured surfaces,[1–5] porous substrates,[6] polymeric liquids,[7] and rarified gases,[8] the breakdown of this commonly used condition has become rather evident. While such slippage is normally thought of as a microscopic effect, in high Reynolds number flows which typically occur at large length scales, its influence might hardly be considered strong enough to change flow characteristics qualitatively. For this reason, it might not seem unreasonable to assume that the behavior of a boundary layer flow with slip does not deviate significantly from its no-slip counterpart. In fact, many existing studies on slipping boundary layer flows have adopted this view by treating the slip merely as minor corrections to the no-slip flow solutions without altering boundary layer structures.[8–11]

However, the impacts of a slip might be not as simple as normally thought because of the following differences between no-slip and slipping boundary layer flows. First, the velocity field of the former, due to the lack of the characteristic length scale, is usually self-similar (except for the situation where the free stream velocity varies with position[12]), whereas the latter generally does *not* possess a self-similar structure because of the additional slip length λ, where λ is defined as the ratio of the fluid velocity (relative to the wall) to the shear rate on the wall. Second, the extent of slip in a boundary layer flow is *not* fixed but varies with λ relative to the boundary layer thickness δ that also varies with the flow speed. These differences imply not only that the standard solution for a no-slip boundary layer flow might not be always adequate to describing a slipping boundary layer flow but also that the additional slip length might alter the boundary layer structure. The latter, in particular, manifests in the strong-slip situation where λ exceeds δ. In this letter, we demonstrate that new boundary layer structures can emerge for such a strong-slip situation.

How wall slip impacts a boundary layer flow starts with the fact that a slipping flow with the driving velocity U actually varies transversely over $\delta + \lambda$ (see Fig. 1), leading the wall stress to $\tau_w \sim \mu U/(\delta + \lambda)$ (with μ being the fluid viscosity), namely,

$$\tau_w \sim (\mu U/\delta)\, S, \tag{1}$$

where $S = \delta/(\delta + \lambda)$ can be deemed as the *drag reduction factor*. For $\delta \gg \lambda$ where slip effects are weak, $S \sim O(1)$ and Eq. (1) recovers the no-slip result $\tau_w \sim \mu U/\delta$. On the other hand, if λ is so large that $\delta \ll \lambda$, the velocity gradient will virtually be across λ, giving $S \sim \delta/\lambda$ and hence $\tau_w \sim \mu U/\lambda$. If the flow is driven by a moving boundary, because not all the momentum from the wall can be transmitted into the fluid, the fluid will move at a speed u *slower* than U. Balancing the corresponding stress $\mu u/\delta$ to (1), we find

$$u \sim S \cdot U, \tag{2}$$

which yields $u \sim U\delta/\lambda$ for $\delta \ll \lambda$ and $u \sim U$ for $\delta \gg \lambda$.

As indicated by Eqs. (1) and (2), both τ_w and u change their scales when $\delta \gg \lambda$ (no-slip limit) switches to $\delta \ll \lambda$ (strong-slip limit), implying distinct boundary layer structures between these two. In the following, we use this idea to analyze two closely related problems in the presence of slip: (i) the Stokes 1st problem and (ii) a steady high Reynolds number

a)Author to whom correspondence should be addressed: hhwei@mail.ncku.edu.tw

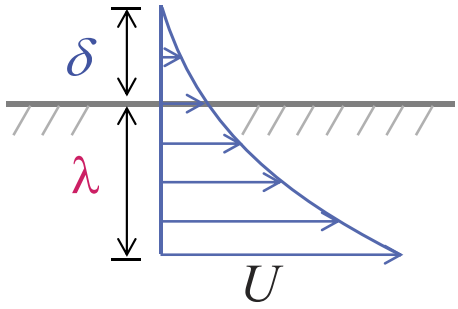

FIG. 1. Schematic picture for a slipping boundary layer flow driven by a moving plate.

boundary layer flow driven by a moving plate, showing that both temporal and spatial structures of boundary layers can undergo qualitative changes due to slip effects.

Consider a transient fluid motion driven by a slippery plate moving at a constant speed U. How the fluid velocity u varies with the distance to the plate y and time t is governed by the diffusion-like momentum equation

$$u_t = \nu u_{yy}, \tag{3}$$

which is subject to the slip condition at the wall ($y = 0$)

$$u - U = \lambda u_y \tag{4}$$

plus $u\,(t = 0) = 0$ and $u\,(y \to \infty) \to 0$. As the viscous boundary layer grows as $\delta \sim (\nu t)^{1/2}$ [via balancing the terms in Eq. (3)], the solution with $\lambda = 0$ takes the well-known form $u/U = \mathrm{erfc}(\eta/2)$ in terms of the self-similar variable $\eta = y/(\nu t)^{1/2}$.[13]

For $\lambda \neq 0$, the situation becomes rather different. For very short times, because $\delta \ll \lambda$, the plate looks very slippery and not much flow can be developed in the fluid, i.e., $u \ll U$. Hence, Eq. (4) can be approximated as $-U \approx \lambda u_y$, making the flow look as if it were driven by a constant wall stress $\tau_w = -\mu u_y\,(y = 0) = \mu U/\lambda$. Since $u_y \sim u/\delta$, the fluid velocity due to this constant stress will scale as $U\delta/\lambda$, similar to Eq. (2) with $\delta \ll \lambda$. Thus, for short times where slip effects are strong, the velocity profile has a very distinct self-similar structure

$$u/U = \left[(\nu t)^{1/2}/\lambda\right] f(\eta), \tag{5a}$$

$$f = \left(2/\pi^{1/2}\right)\exp\left(-\eta^2/4\right) - \eta\,\mathrm{erfc}(\eta/2). \tag{5b}$$

Here (5b) can be obtained by an integration of the transformed equation of Eq. (3) $f - \eta f' = 2f''$ with $f'(0) = -1$ (owing to $-U \approx \lambda u_y$) and $f(\infty) = 0$.

In fact, the strong-slip velocity profile Eq. (5) can be obtained from a vorticity point of view by solving for the vorticity distribution $\omega = -u_y$ corresponding to (3) and (4) $\omega_t = \nu\omega_{yy}$ and $\omega\,(y = 0) = U/\lambda$. So the problem becomes exactly the Stokes 1st problem for vorticity that is generated from the virtual no-slip plane below the wall. Together with $\omega(t = 0) = 0$ and $\omega\,(y \to \infty) = 0$, the solution is $\omega = (U/\lambda)\,\mathrm{erfc}(\eta/2)$, whose integration gives exactly Eq. (5).

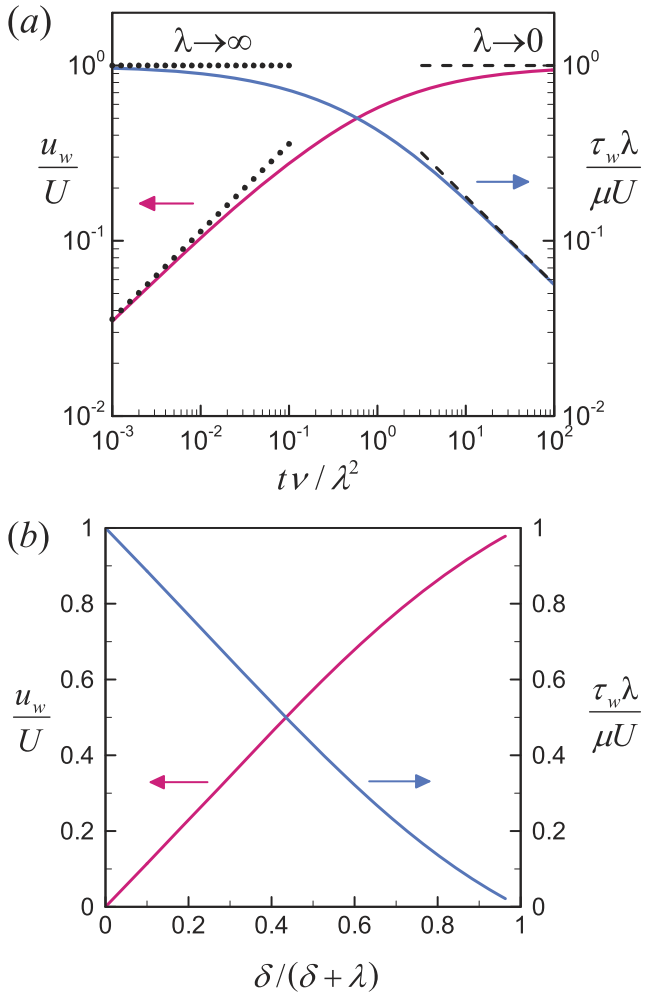

FIG. 2. (a) Temporal responses for the wall velocity u_w and stress τ_w using the exact solution obtained in Ref. 14. Short-term and long-term responses follow $\lambda \to \infty$ (dotted lines) and $\lambda \to 0$ (dashed lines) results, respectively, with a crossover at $t \sim \lambda^2/\nu$. (b) Replot of (a), showing that both u_w and τ_w vary virtually linearly with $\delta/(\delta + \lambda)$, confirming the universal scalings (2) and (1).

As for long times, because $\delta \gg \lambda$, the slip term in Eq. (4) becomes negligible. Hence $u(\sim U)$ can be described by the usual no-slip solution to give the wall stress $\tau_w \sim \mu U/\delta \sim \mu U/(\nu t)^{1/2}$. Both short and long time responses crossover at time $t \sim \lambda^2/\nu$—the viscous diffusion time across the slip length when $\delta \sim (\nu t)^{1/2}$ grows to the size of λ. It also marks the unique time scale for the onset of the *slip-to-slick transition* (SST).

Using the exact solution obtained in Ref. 14, we plot temporal responses for the wall velocity u_w and stress τ_w in Fig. 2(a), showing that the short-term and long-term responses do correspond to the strong-slip and no-slip results, respectively. In fact, Fig. 2(b) reveals that both τ_w and u_w vary virtually linearly with $S = \delta/(\delta + \lambda)$, confirming the universal scalings (1) and (2).

In analogy to the Stokes 1st problem, a similar flow structure change can also occur *spatially* to a steady boundary layer flow driven by a moving slippery plate (of length L). This moving boundary problem can be used to model sheet

drawing or fiber extrusion processes.[15] Let u and v denote the velocity components in the streamwise (in x) and transverse (in y) directions, respectively. The equations governing the flow field within the boundary layer are

$$u_x + v_y = 0, \tag{6a}$$

$$uu_x + vu_y = \nu u_{yy}, \tag{6b}$$

subject to the slip condition Eq. (4) $u - U = \lambda u_y$ and $v = 0$ at the plate ($y = 0$) plus $u(y \to \infty) = 0$.

At low U (but still in the high Reynolds number regime) such that $\delta \gg \lambda$, the slip condition (4) is reduced to the usual no-slip condition $u \approx U$. Balancing the inertial terms $\sim U^2/x$ to the viscous term $\sim \nu U/\delta^2$ in Eq. (6b), we recover the well-known Blasius boundary layer scale

$$\delta \sim (\nu x/U)^{1/2} \equiv \delta_B(x) \tag{7a}$$

or

$$\delta_B(x = L) = LRe^{-1/2}, \tag{7b}$$

where $Re = UL/\nu$ is the Reynolds number. A self-similar solution can then be constructed as $u/U = f'(\eta)$ with $\eta = y/\delta_B(x)$, reducing Eq. (6) to $ff' + 2f''' = 0$ with $f'(0) = 1$, $f(0) = 0$, and $f'(\infty) = 0$.[15] We are interested in the overall skin friction coefficient which is defined as

$$C_f = \left(\int_0^L \tau_w dx/L\right) \Big/ \left(\rho U^2/2\right). \tag{8}$$

With the wall stress $\tau_w = -\mu U f''(0)/\delta_B$, Eq. (8) yields the well-known $-1/2$ law

$$C_f = 4|f''(0)|Re^{-1/2}, \tag{9}$$

with $f''(0) = -0.443\,75$.[15]

The Blasius scale (7) indicates that increasing U will thin δ as $\delta \propto U^{-1/2}$. This means that if U increases to the point where δ is comparable to or thinner than λ, the classical no-slip results given above will cease to hold. In particular, if U is sufficiently high (but still in the laminar regime) such that $\delta \ll \lambda$, $u \sim (\delta/\lambda)U \ll U$ in Eq. (4) and the fluid at the wall will slide according to $-U \approx \lambda u_y$. Balancing the inertial terms $\sim(\delta/\lambda)^2 U^2/x$ to the viscous term $\sim \nu(\delta/\lambda)U/\delta^2$ in Eq. (6b), we find a new scaling for δ,

$$\delta \sim (\nu\lambda x/U)^{1/3} \equiv \delta_s(x) \tag{10a}$$

or

$$\delta_s(x = L) = LRe^{-1/3}(\lambda/L)^{1/3}. \tag{10b}$$

Also because of (10), the velocity profile will take a new self-similar form

$$u/U = (\delta_s(x)/\lambda)\phi'(\eta) \text{ with } \eta = y/\delta_s(x), \tag{11}$$

where ϕ is determined by the ordinary differential equation transformed from Eq. (6),

$$(\phi')^2 - 2\phi\phi'' = 3\phi''', \tag{12}$$

with $\phi''(0) = -1$, $\phi(0) = 0$, and $\phi'(\infty) = 0$. A more formal way to derive this new boundary layer structure is given in the supplementary material. As the wall stress here is simply $\tau_w = \mu U/\lambda$, the corresponding skin friction coefficient (8) becomes

$$C_f = 2(L/\lambda)Re^{-1}. \tag{13}$$

It is similar to Levich's free-surface result $C_f \sim Re^{-1}$.[16] Direct numerical simulations do show that C_f can be reduced to Levich's free-surface result as $\lambda \to \infty$.[17] But here, we show that for a finite value of λ, it must enter to characterize the boundary layer flow.

Because the no-slip $-1/2$ law (9) for $\delta \gg \lambda$ at low U can turn into the strong-slip -1 law (13) for $\delta \ll \lambda$ at high U, the change will occur at the crossover Reynolds number between these two laws,

$$Re_c \sim (L/\lambda)^2, \tag{14}$$

which also marks the SST point from the no-slip Blasius scaling (7b) to the strong-slip scaling (10b) for δ.

In fact, just like the Stokes 1st problem, both no-slip and strong-slip cases can be unified using Eq. (2). Letting $x \sim L$ and balancing the inertial terms $\sim S^2U^2/L$ to the viscous term $\sim \nu SU/\delta^2$ in Eq. (6b), we find

$$\delta/L \sim S^{-1/2}Re^{-1/2}, \tag{15}$$

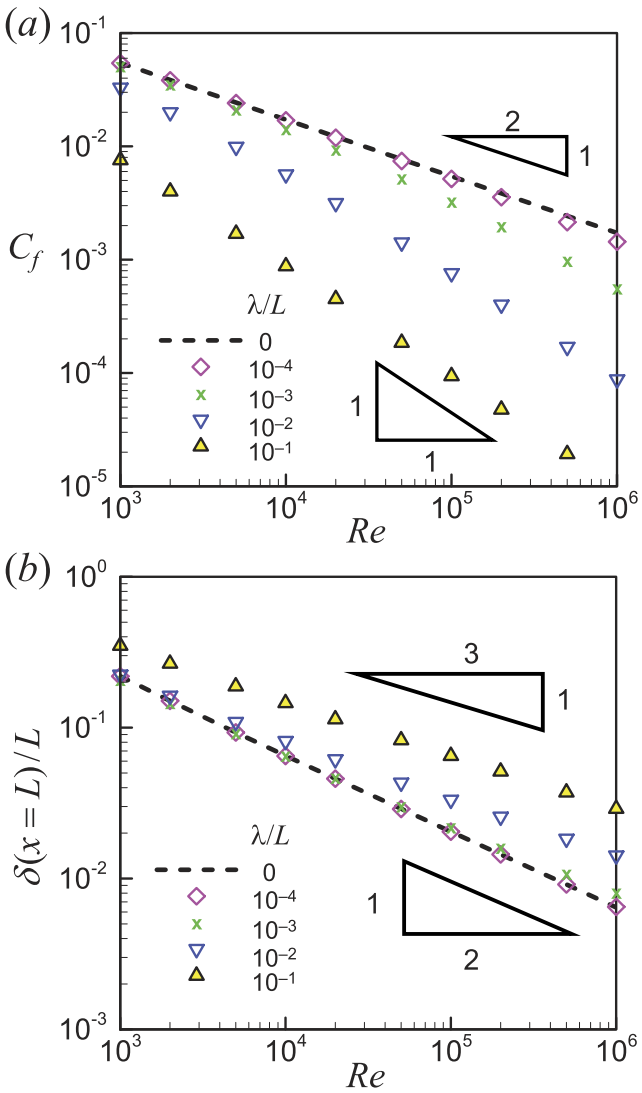

FIG. 3. (a) Plot of C_f against Re for various values of λ/L, showing that the friction law can change from the no-slip $-1/2$ law (9) to the strong-slip -1 law (13) when increasing λ from small to large values. (b) Plot of $\delta(x = L)/L$ against Re to show the corresponding scaling changes for δ, revealing that δ can change from $-1/2$ law (7b) to the $-1/3$ law (10b).

which is able to unify both the no-slip −1/2 law (7b) for $\delta \gg \lambda$ and the strong-slip −1/3 law (10b) for $\delta \ll \lambda$. Using $C_f \sim \tau_w/\rho U^2 \sim L/(\delta+\lambda)\cdot Re^{-1}$ and setting $\delta \sim \delta_B = LRe^{-1/2}$, the two distinct friction laws (9) and (13) can also be unified as $C_f \sim Re^{-1/2}/[Re^{1/2}(\lambda/L)+1]$. Recognizing $C_f\,(\lambda=0) \sim Re^{-1/2}$ from Eq. (9), the above universal friction relationship can be re-written as

$$C_f/C_f(\lambda=0) \sim 1/\left[Re^{1/2}(\lambda/L)+1\right], \tag{16}$$

which signifies an apparent drag reduction when increasing Re beyond the SST point $Re_c \sim (L/\lambda)^2$ given by (14). The friction relationship (16) also agrees with that given in Ref. 18.

To test our scaling results described above, we solve Eq. (6) numerically using prediction and correction iteration scheme[19] in conjunction with the up-wind scheme for discretizing the inertial terms. Figure 3(a) plots C_f against Re for various values of λ/L. The result clearly shows that the friction law can shift from the no-slip −1/2 law (9) to the strong-slip −1 law (13) when gradually increasing the value of λ/L. The corresponding scaling change for δ can be seen by plotting $\delta(x=L)/L$ against Re. As shown in Fig. 3(b), the change from the no-slip −1/2 law (7b) to the strong-slip −1/3 law (10b) is also evident.

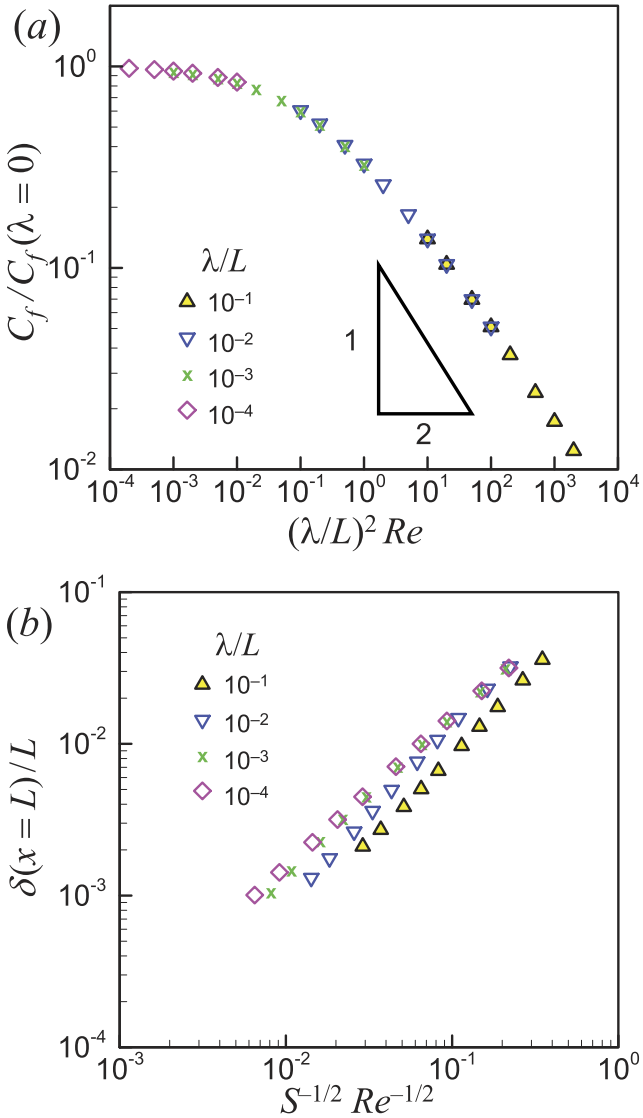

FIG. 4. (a) The no-slip −1/2 friction law (9) and the strong slip −1 friction law (13) can be collapsed according to (16). The transition between these two laws occurs at $(\lambda/L)^2\,Re \sim 1$, in agreement with (14). (b) The corresponding −1/2 law (7b) and −1/3 law (10b) for δ seen in Fig. 3(b) can be unified as $\delta/L \sim S^{-1/2}\,Re^{-1/2}$ according to (15), where $S = \delta/(\delta+\lambda)$.

Figure 4(a) shows that the two distinct friction laws (9) and (13) can be collapsed according to the universal friction law (16), with the transition at $(\lambda/L)^2 Re \sim 1$ as predicted by Eq. (14). The corresponding scaling laws for δ: (7b) and (10b) also virtually collapse according to the universal boundary layer law (15), as shown in Fig. 4(b). All these numerical results confirm the scaling changes shown earlier. We emphasize that the universal laws (15) and (16) can describe any situation with an arbitrary extent of slip λ/δ, including the situation near the SST in which $\lambda/\delta \sim O(1)$ and the flow is *not* self-similar.

We also expect that a similar flow characteristic change can also occur to a flow past a *fixed* plate. This fixed plate situation is in fact a special case of the Falkner-Skan boundary layer flow over wedge. In the latter case, the external flow outside the boundary layer is *irrotational* and takes the form $U_e(x) = U_0\,(x/L)^m$,[13] where L and U_0 stand for the characteristic length and velocity scales, respectively, and $m = \beta/(2-\beta)$ is the exponent depending on the wedge angle $\beta\pi$. The governing equations for this flow are Eq. (6a) plus the following momentum equation:

$$uu_x + vu_y = U_eU_e' + \nu u_{yy}, \tag{17}$$

where $U_eU_e' = m(U_0^2/L)\,(x/L)^{2m-1}$ comes from the Bernoulli pressure with $U_e' \equiv dU_e/dx$. Boundary conditions are $u = \lambda u_y$ at $y=0$ and $u\,(y\to\infty) = U_e$.

In the no-slip limit ($\delta \gg \lambda$), just like a uniform flow over a flat plate, how the boundary layer here varies with x simply follows the Blasius scaling (7a) with U being replaced by $U_e(x)$,

$$\delta_F(x) = LRe_0^{-1/2}(x/L)^{(1-m)/2}, \tag{18}$$

with $Re_0 = U_0L/\nu$. The velocity profile can then be constructed as $u = U_e(x)\,f'(\eta)$ with $\eta = y/\delta_F(x)$, and f can be determined from the transformed equation of Eq. (17): $f''' + [(m+1)/2]\,ff'' + m\,(1-f'^2) = 0$ with $f'(0) = 0$, $f(0) = 0$, and $f'(\infty) = 1$. The skin friction coefficient (8) can be determined as

$$C_f = 4f''(0)/(3m+1)\cdot Re_0^{-1/2}. \tag{19}$$

Obviously, $m = 0$ reduces to the classical Blasius result.

In the strong-slip limit ($\delta \ll \lambda$), we set $u = U_e(x) + \tilde{u}$ with $\tilde{u}$ being the correction to the local plug flow, i.e., $|\tilde{u}| \ll U_0$. Substituting the above into Eq. (17) and dropping higher order terms $\tilde{u}\tilde{u}_x$ and $v\tilde{u}_y$, we get

$$(U_e\tilde{u})_x = \nu\tilde{u}_{yy}, \tag{20}$$

subject to $u(y\to\infty) = U_e$ and the strong-slip conditon $U_e = \lambda\tilde{u}_y$ at $y=0$. In this case, while the boundary layer thickness still scales as (18), the flow has the following self-similar structure due to constant shearing set up by the above strong-slip condition:

$$\widetilde{u} = [\delta_F(x)/\lambda]U_e(x)F(\eta) \text{ with } \eta = y/\delta_F(x), \tag{21}$$

where F is determined by the following equation after substituting (21) into (20):

$$2F'' + (1-m)\eta F' - (1+3m)F = 0, \tag{22}$$

with $F'(0) = 1$ and $F(\infty) = 0$. Since the local flow field is a plug flow, the resulting wall shear stress is $\tau_w = \mu U_e(x)/\lambda$, leading the skin friction coefficient (8) to

$$C_f = 2/(m+1) \cdot (L/\lambda) {Re_0}^{-1}. \tag{23}$$

Again, C_f still changes from ${Re_0}^{-1/2}$ to ${Re_0}^{-1}$ when increasing Re_0 beyond the SST point $\sim(L/\lambda)^2$ at the crossover between (19) and (23).

The key feature of a slipping boundary layer flow is that the extent of the wall slip is not fixed but varies with the boundary layer thickness δ. This leads to a slip-stick transition and a flow characteristic change when δ becomes comparable to or thinner than the slip length λ.The present analysis is merely restricted to simple boundary layer flows and we demonstrate that new self-similar boundary layer structures can arise from wall slip. Such new structures can likely be seen in boundary layer flows over superhydrophobic plates[5,18] or porous substrates[20] in which effective slip lengths can be of μm or larger due to trapped air bubbles or fluid leakage on surfaces. A similar flow characteristic change might also occur in weakly rarefied gas flows in small MEMS devices or in low pressure applications where large boundary slip can exist.[21] For liquid flows, the extent of slip could be relatively small owing to relatively thick boundary layers. In this case, the distinct temporal responses found for the Stokes 1st problem could be used to experimentally determine slip lengths using an oscillatory rheometer.

For non-similar boundary layer flows which are more prevalent in practice, we expect that they might also undergo similar flow characteristic changes like those reported here. In any case, such flow characteristic changes can have profound impacts on convective heat or mass transfer processes. Taking a flow over a fixed slippery plate as an example, the Nusselt number Nu will be increased by increasing the amount of wall slip, changing the no-slip result $Nu \sim Re^{1/2}\, Pr^{1/3}$ to the strong-slip or free-surface result $Nu \sim Re^{1/2}\, Pr^{1/2}$,[13] where Pr is the Prandtl number. On the contrary, if the plate is moving as in a sheet drawing process, Nu will be *diminished* by slip and its strong-slip behavior will be completely different from the fixed plate case because of (10). As all these characteristic changes are exclusive to the situation where wall slip is present; they might provide new alternatives for probing slip boundaries or for a better control of transports in wall-bounded boundary layer flows.

While the present work merely focuses on how slip modifies the characteristics of a boundary layer flow in the laminar regime, our findings might provide renewed insights into its subsequent development to turbulence. Recent studies reveal that slip effects arising from surface structure and hydrophobicity can significantly alter the behavior of turbulent boundary layer flows.[18,22–25] Such development, which is still waiting for exploration, might have strong connections to the features found in these studies.

See supplementary material for the formal derivations of Eqs. (10)–(12).

This work was supported by the Ministry of Science and Technology of Taiwan under Grant No. 105-2221-E-006-227-MY3 of H.H.W.

[1] D. C. Tretheway and C. D. Meinhart, "Apparent fluid slip at hydrophobic microchannel walls," Phys. Fluids **14**, L9 (2002).
[2] C. Lee, C.-H. Choi, and C.-J. Kim, "Structured surfaces for a giant liquid slip," Phys. Rev. Lett. **101**, 064501 (2008).
[3] R. J. Daniello, N. E. Waterhouse, and J. P. Rothstein, "Drag reduction in turbulent flows over superhydrophobic surfaces," Phys. Fluids **21**, 085103 (2009).
[4] P. Tsai, A. M. Peters, C. Pirat, M. Wessling, R. G. H. Lammertink, and D. Lohse, "Quantifying effective slip length over micropatterned hydrophobic surfaces," Phys. Fluids **21**, 112002 (2009).
[5] E. Aljallis, M. A. Sarshar, R. Datla, V. Sikka, A, Jones, and C.-H. Choi, "Experimental study of skin friction drag reduction on superhydrophobic flat plates in high Reynolds number boundary layer flow," Phys. Fluids **25**, 025103 (2013).
[6] G. S. Beavers and D. D. Joseph, "Boundary conditions at a naturally permeable wall," J. Fluid Mech. **30**, 197–207 (1967).
[7] F. Brochard-Wyart, P.-G. DeGennes, H. Hervert, and C. Redon, "Wetting and slippage of polymer melts on semi-ideal surfaces," Langmuir **10**, 1566–1572 (1994).
[8] M. J. Martin and I. D. Boyd, "Momentum and heat transfer in a laminar boundary layer with slip flow," J. Thermophys. Heat Transfer **20**, 710–719 (2006).
[9] H. Hasimoto, "Boundary-layer slip solutions for a flat plate," J. Aerosp. Sci. **25**, 68–69 (1958).
[10] C. Y. Wang, "Flow due to a stretching boundary with partial slip—An exact solution of the Navier–Stokes equations," Chem. Eng. Sci. **57**, 3745–3747 (2002).
[11] A. Aziz, "Hydrodynamic and thermal slip flow boundary layers over a flat plate with constant heat flux boundary condition," Commun. Nonlinear Sci. Numer. Simul. **15**, 573–580 (2010).
[12] E. M. Sparrow, H. Quack, and C. J. Boerner, "Local nonsimilarity boundary-layer solutions," AIAA J. **8**, 1936–1942 (1970).
[13] L. G. Leal, *Laminar Flow and Convective Transport Processes* (Butterworth-Heinemann, Boston, 1992).
[14] M. T. Matthews and J. M. Hill, "On three simple experiments to determine slip lengths," Microfluid. Nanofluid. **6**, 611–619 (2009).
[15] B. C. Sakiadis, "Boundary-layer behavior on continuous solid surfaces: II. The boundary layer on a continuous flat surface," AIChE J. **7**, 221–225 (1961).
[16] V. G. Levich, "The motion of gas bubbles at high Reynolds numbers," Zh. Eksp. Teor. Fiz. **19**, 18–24 (1949) (in Russian).
[17] G. H. Atefi, H. Niazmand, and M. R. Meigounpoory, "Numerical analysis of 3-d flow past a stationary sphere with slip condition at low and moderate Reynolds numbers," J. Dispersion Sci. Technol. **28**, 591–602 (2007).
[18] C. C. Mei and X. Y. Guo, "Numerical study of laminar boundary-layer flows over a superhydrophobic plate," Phys. Fluids **30**, 072002 (2018).
[19] S. V. Patankar, *Numerical Heat Transfer and Fluid Flow* (Hemisphere, London, 1980).
[20] K. A. Nair and A. Sameen, "Experimental study of slip flow at the fluid-porous interface in a boundary layer flow," Procedia IUTAM **15**, 293–299 (2015).
[21] M. Gad-el-Hak, "The fluid mechanics of microdevices−the Freeman scholar lecture," J. Fluids Eng. **121**, 5–33 (1999).
[22] T. O. Jelly, S. Y. Jung, and T. A. Zaki, "Turbulence and skin friction modification in channel flow with streamwise-aligned superhydrophobic surface texture," Phys. Fluids **26**, 095102 (2014).
[23] J. Seo and A. Mani, "On the scaling of the slip velocity in turbulent flows over superhydrophobic surfaces," Phys. Fluids **28**, 025110 (2016).
[24] B. J. Rosenberg, T. V. Buren, M. K. Fu, and A. J. Smits, "Turbulent drag reduction over air- and liquid- impregnated surfaces," Phys. Fluids **28**, 015103 (2016).
[25] W. A. Rowin, J. Hou, and S. Ghaemi, "Inner and outer layer turbulence over a superhydrophobic surface with low roughness level at low Reynolds number," Phys. Fluids **29**, 095106 (2017).